Image Processing: Algorithms and Systems IV, San Jose, California, USA, 16–20 January 2005, Proc. SPIE 5672

Sampling the Parameter Domain of Image Series

Michael Heizmann and Jürgen Beyerer

Fraunhofer IITB Institut Informations- und Datenverarbeitung,
Fraunhoferstraße 1, D-76131 Karlsruhe, Germany

ABSTRACT

While analyzing a scene of interest in real environments, the acquisition and evaluation of image series has proven to yield promising results in providing useful information. However, acquiring and evaluating image series imposes several difficulties on the imaging and analysis process: The amount of data to be processed increases significantly, especially when more than one parameter is varied. Recording image series thus leads to a dilemma: Whereas a dense scanning of the varied parameter is desirable in order not to lose any information of interest, the number of recorded images should be as small as possible to ensure both adequate acquisition time and manageable amount of data. This dilemma can be considered as a sampling issue of the parameter spaces of a variable image acquisition. In this contribution, the topic of optimally sampling the parameter spaces for image series is addressed from a practical point of view. Sampling conditions for several parameters to be varied are derived from physics and image formation models.

Keywords: Automated visual inspection, image series, image processing, image fusion, reflection models, sampling theorem.

1. INTRODUCTION

In automated visual inspection, a research area of great interest is made up of variable acquisition techniques. An important subarea comprises the utilization of robots as sensor manipulators, e. g. in order to extend the field of view for a camera. Furthermore, extra information on a scene, which otherwise would have to be registered with additional effort and supplementary measurement devices, can be retrieved through fusing image series recorded while image formation parameters are varied. Such fast and non-contacting information sources may provide interesting opportunities to the users of automated visual inspection systems.

In order to obtain an image, three principal components are needed: the scene (or the object) of interest, the observer (usually a camera), and the illumination. Given an image retrieval environment, the appearance of a scene is fully defined through the arrangement and the characteristics of the observer and the illumination. These degrees of freedom of the image recording play the role of parameters for the acquisition process. When a static scene is considered, the distribution of radiation on the imaging sensor is fixed by a given parameter set. Consequently, two images recorded with the same acquisition parameters will only differ by the noise of the imaging sensor.

In contrast to usual scenes in environmental observation (e. g. military reconnaissance, driver assistance), most imaging conditions in industrial visual inspection are controllable. In the former case, the image application and evaluation has to manage with images recorded by a more or less fix constellation of acquisition. In most cases, such camera systems use passive sensors without additional illumination. The arrangement of the illumination is thus static, and the point of view is given by the position of the sensor platform or vehicle. In consequence, image processing for reconnaissance and driver assistance is usually optimized to extract the optimum of information from single images, whereas automated visual systems for industrial applications may benefit from systematic variations of the image formation.

Further author information:
E-mail: {heizmann, beyerer}@iitb.fraunhofer.de; WWW: www.iitb.fraunhofer.de, www.ies.uni-karlsruhe.de;
Telephone: +49-721-6091-{329, 210}; Fax: +49-721-6091-413

2. SAMPLING OF PARAMETERS

The basic understanding of the principles of sampling, i. e. converting a continuous function $f(x)$ into a sequence of values f_k, goes back to Shannon, Whittacker and Kotel'nikov.[1,2] Shannon's theorem states that $f(x)$ is completely determined by the sequence $f(x_k)$, if $f(x)$ is bandlimited by $\omega_{\max}$ and the $f(x_k)$ are the values of $f(x)$ at $x_k = kT$ with the sampling interval $T \leq \frac{\pi}{\omega_{\max}}$. The reconstruction $\tilde{f}(x)$ is then obtained by interpolating the sequence with

$$\tilde{f}(x) = \sum_{k \in \mathbb{Z}} f(x_k) \cdot \operatorname{sinc}\left(\frac{x}{T} - k\right) \ , \tag{1}$$

where $\operatorname{sinc}(x) = \frac{\sin(\pi x)}{\pi x}$. Given a sampling interval T, the corresponding maximum frequency of $f(x)$ that allows a complete reconstruction is the Nyquist frequency $\omega_{\max} \leq \omega_{\text{Nyquist}} = \frac{\pi}{T}$.

The sampling theorem is fully applicable to the acquisition of image series. Here, the image signal is not predominantly treated as a function of the position $\boldsymbol{x}$, but as a function $f_{\boldsymbol{x}}(\xi_i)$ of image intensities for each image point $\boldsymbol{x}$ with respect to the parameter ξ_i. Obviously, the sampling theorem has to be satisfied for each parameter ξ_i in order to maintain the correct characteristic of the image intensity, when its dependency on ξ_i is considered. In this context, the spectral properties of the imaging parameters play a crucial role: On the one hand, parameters which lead to abrupt changes in the received intensity need a careful variation and a fine sampling. On the other hand, parameters which are known to cause only slight intensity changes or intensity curves comprising only the first harmonic component can be recorded using only few sampling points. Therefore, Sects. 3 and 4 list and characterize some important imaging parameters. In Sect. 5, it will be shown that reflection modelling can lead to detailed previous knowledge on the image intensities to be expected.

A more general understanding of sampling starts from the development of the function in question $f(x)$ in an orthonormal basis.[2] $f(x)$ is assumed to be a real signal of finite energy and hence belongs to L_2, the space of square integrable functions. L_2 is a Hilbert-Space. Its norm is induced by the standard scalar product:

$$\langle f, g \rangle = \int_{-\infty}^{+\infty} f^*(x)\, g(x)\, \mathrm{d}x \ . \tag{2}$$

In a normalized form ($T = 1$), Eq. (1) can be written as

$$f(x) = \sum_{k \in \mathbb{Z}} c(k)\ \varphi_k \ , \tag{3}$$

where the functions $\varphi_k = \operatorname{sinc}(x - k)$ are the basis functions of an orthonormal basis, since

$$\langle \varphi_k, \varphi_l \rangle = \begin{cases} 1 \ , & k = l \ , \\ 0 \ , & k \neq l \ , \end{cases} \tag{4}$$

and the $c(k)$'s are coefficients in this basis. The projection of the L_2-function $f(x)$ on the subspace of bandlimited functions V is then obtained with the orthogonal projection operator $\mathcal{P}_V : L_2 \to V$ with

$$\mathcal{P}_V f = \sum_{k \in \mathbb{Z}} \langle f, \varphi_k \rangle\, \varphi_k \ . \tag{5}$$

Unfortunately, the interpretation of sampling as a development of $f(x)$ in such orthonormal basis functions imposes several problems to our application:

- The sinc-basis used in Eq. (3) is incomplete for non-bandlimited functions. They fail to span all of L_2. In general, the intensity signals $f_{\boldsymbol{x}}(\xi_i)$ are not necessarily bandlimited. An example is given by the impulse function, which is closely related to specular reflection introduced in Sect. 5.1.
- When non-bandlimited functions are processed, the projection in Eq. (5) leads to an approximation error. In this case, the scalar product of Eq. (3) corresponds to a convolution with the sinc-function and thus with an ideal low-pass filtering. If the basis is orthonormal, the projection can be shown to yield the minimum-error approximation of f in V.[3]

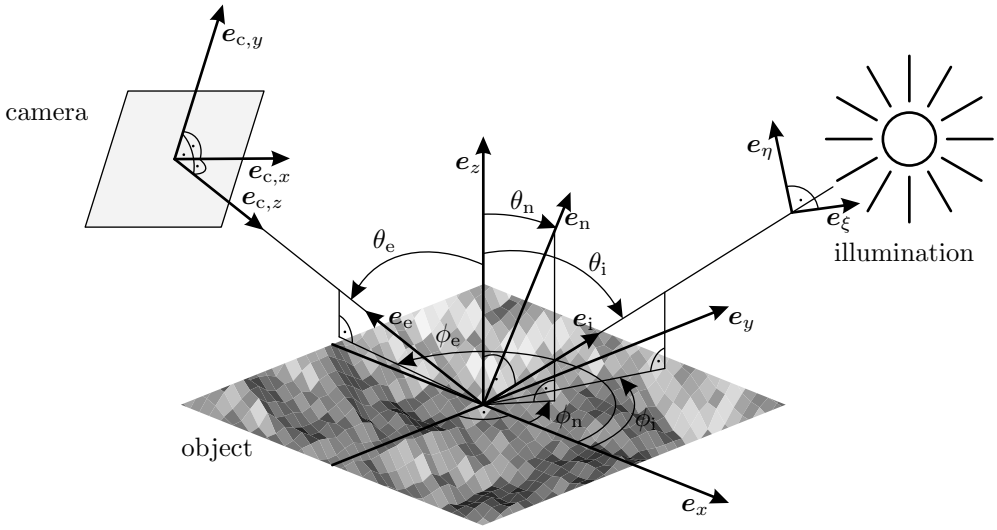

Figure 1. Principal characterization of illumination and imaging.

- An additional drawback arises with spherical or hemispherical parameter domains like the illumination and observation angles (θ_i, ϕ_i and θ_e, ϕ_e): The basis functions for spherical domains are obtained by Legendre polynomials.[4] Here, an angularly equidistant sampling is only obtained for some special cases (namely for $N = (\kappa+1)^2$, $\kappa \in \mathbb{N}$ sampling points). Even in these cases, the resulting basis functions are not necessarily orthogonal for any κ. In consequence, an additional error occurs at the projection of f onto such a non-orthonormal basis.

In consequence, major difficulties arise when such theoretical sampling conditions are to be transferred into practical recording instructions. When even more parameters must be considered simultaneously, an exact deduction of the sampling conditions from the underlying basis functions of the parameter space can hardly be handled. In such cases, an alternative way of deriving suitable sampling conditions is possible, when assumptions can be made on the signal to be observed. Such an approach depends on a comprehensive understanding of the physics involved in image formation. Moreover, appropriate models of the surface reflection can be used to infer adequate sampling instructions. In the following sections, parameter characteristics are used to specify conditions for some exemplary imaging parameters. It will be shown that modelling the light reflection process can be used to legitimate a reasonable sampling.

3. IMAGING PARAMETERS

Acquisition parameters can be divided in illumination properties and camera parameters, see Fig. 1 and Tab. 1. Among these, the geometrical parameters are referred to a global coordinate system, which is chosen with an average normal $\boldsymbol{e}_z$ of a rough object surface. The object surface $\boldsymbol{x} = (x, y, z)^\mathrm{T}$ is defined explicitly as $z = f(x, y)$, and the resulting local surface normal is obtained to $\boldsymbol{e}_\mathrm{n} = (\cos\phi_\mathrm{n} \sin\theta_\mathrm{n}, \sin\phi_\mathrm{n} \sin\theta_\mathrm{n}, \cos\theta_\mathrm{n})^\mathrm{T} \propto (\frac{\partial z}{\partial x}, \frac{\partial z}{\partial y}, 1)^\mathrm{T}$.

The illumination is modelled by a linear superposition of some remote point sources. They can be characterized with their viewing direction $\boldsymbol{e}_\mathrm{i} = (\cos\phi_\mathrm{i} \sin\theta_\mathrm{i}, \sin\phi_\mathrm{i} \sin\theta_\mathrm{i}, \cos\theta_\mathrm{i})^\mathrm{T}$ from the surface point and the spectral irradiance $E_{\mathrm{i},\lambda} = \frac{\partial E_\mathrm{i}}{\partial \lambda}$. For the polarization state of the illuminating light, two orthogonal oscillating planes have to be chosen. In our case, they are spanned by the vectors $\boldsymbol{e}_\mathrm{i}$, $\boldsymbol{e}_\xi$ and $\boldsymbol{e}_\mathrm{i}$, $\boldsymbol{e}_\eta$ with $(\boldsymbol{e}_z \times \boldsymbol{e}_\mathrm{i}) \cdot \boldsymbol{e}_\eta = 0$, $\boldsymbol{e}_\mathrm{i} \cdot \boldsymbol{e}_\xi = 0$, and $\boldsymbol{e}_\mathrm{i} \cdot \boldsymbol{e}_\eta = 0$. The electromagnetic wave contains then the components $E_{\mathrm{i},\xi}$ and $E_{\mathrm{i},\eta}$ and can be formulated[5] with the vector of the electrical field $\boldsymbol{E}_\mathrm{i} = E_{\mathrm{i},\xi} \cos(\tau + \delta_\xi)\boldsymbol{e}_\xi + E_{\mathrm{i},\eta} \cos(\tau + \delta_\eta)\boldsymbol{e}_\eta$, where $\Delta\delta_\mathrm{i} = \delta_\eta - \delta_\xi$ denotes the phase shift of the oscillation. Additional degrees of freedom are given by the coherence of the light waves, described e. g. by the frequency bandwidth $\Delta\nu \propto \frac{1}{\Delta\lambda}$ of the light source.[6]

For the image acquisition system, a simplified orthographic projection is assumed in this contribution. This simplification is acceptable, if the distance between the object and the camera is large compared to the object size

Table 1. Imaging parameters.

Parameter	Cyclicity	Support
Illumination		
Azimuth ϕ_i	yes	$[0; 2\pi)$
Polar angle θ_i	no	$[0; \frac{\pi}{2}]$
Spectrum $E_{\mathrm{i},\lambda}$	no	unlimited (usually limited to the visible range $\approx [400\,\mathrm{nm}; 800\,\mathrm{nm}]$)
Polarization state		
Maximum amplitude $E_{\mathrm{i},\xi}$	no	≥ 0
Maximum amplitude $E_{\mathrm{i},\eta}$	no	≥ 0
Phase shift $\Delta\delta_\mathrm{i}$	yes	$[0; 2\pi)$
Intensity $I_\mathrm{lin}(\chi)$ (derived)	yes	$\chi \in [0; \pi)$
Intensity $I_\mathrm{circ}(\chi)$ (derived)	yes	$\chi \in [0; \pi)$
Spatial intensity distribution	yes (for cyclic illumination patterns)	$\mathbb{R}^2$
Coherence $\Delta\nu$	no	
Camera		
Azimuth ϕ_e	yes	$[0; 2\pi)$
Polar angle θ_e	no	$[0; \frac{\pi}{2})$
Polarization state		
Maximum amplitude $E_{\mathrm{c},x}$	no	≥ 0
Maximum amplitude $E_{\mathrm{c},y}$	no	≥ 0
Phase shift $\Delta\delta_\mathrm{c}$	yes	$[0; 2\pi)$
Intensity $I_{\mathrm{c,lin}}(\chi)$ (derived)	yes	$\chi \in [0; \pi)$
Intensity $I_{\mathrm{c,circ}}(\chi)$ (derived)	yes	$\chi \in [0; \pi)$
Aperture ω_c	no	$[0; 2\pi)$
Camera distance	no	$[0; \infty)$
Camera orientation: roll	yes	$[0; 2\pi)$
Intrinsic parameters	no	
Focus distance	no	$[0; \infty)$

and focussing issues are neglected. In this approximation, the camera is characterized by the azimuth ϕ_c and the polar angle θ_c. The alignment of the image borders is chosen to comply with the condition $(\boldsymbol{e}_z \times \boldsymbol{e}_\mathrm{c}) \cdot \boldsymbol{e}_{\mathrm{c},y} = 0$, which fixes the roll angle of the camera. The image formation of the object leads to a received intensity $I(x_\mathrm{c}, y_\mathrm{c})$ on the camera sensor which is proportional to $L(x, y, z, \theta_\mathrm{e}, \phi_\mathrm{e})$, the emitted radiance of the object. By analogy with the illumination, the polarization state of the light reflected from the object is described with $\boldsymbol{E}_\mathrm{c} = E_{\mathrm{c},x} \cos(\tau + \delta_{\mathrm{c},x})\boldsymbol{e}_{\mathrm{c},x} + E_{\mathrm{c},y} \cos(\tau + \delta_{\mathrm{c},y})\boldsymbol{e}_{\mathrm{c},y}$ and $\Delta\delta_\mathrm{c} = \delta_{\mathrm{c},y} - \delta_{\mathrm{c},x}$. To obtain a complete parameter list, Tab. 1 contains the remaining camera parameters that are needed for a perspective camera model.[7] In addition to the common six extrinsic and intrinsic parameters, the focus distance and aperture are important acquisition parameters, which can be used e. g. for focus series acquisition and variations of the focus depth.

In automated visual inspection, variations of some of the imaging parameters have been successfully applied.

For example, the variation of the illumination direction has been applied to obtain topographical information on a given scene.[8] For perfectly diffuse (Lambertian) surfaces, the surface orientation and the respective reflectance factor can be determined from three recordings, provided that they have been taken with point light sources with identical irradiances at the object position and that the illuminations directions do not lie in a plane. When more specialized models of surface reflections are to be considered, the amount of images needed can even be reduced to two images. Such photometric stereo methods can be implemented by introducing reflectance maps that describe the image irradiance as a function of the surface normal for a given illumination direction and a given model of surface reflection. Although three illuminations are theoretically sufficient to determine the surface orientation for Lambertian surfaces, the choice of the illumination direction, mainly the phase angle $\angle(\boldsymbol{e}_\mathrm{i};\boldsymbol{e}_\mathrm{e})$, plays a crucial role for the achievable accuracy. The orientation uncertainties can vary significantly, when the same measurement error of the image irradiances is assumed.[8] These uncertainties can be reduced by taking more than the theoretically necessary number of images.[9]

Another technique for applying variable illumination with respect to the azimuth uses contrast differences in anisotropic surfaces for texture segmentation.[10] For groove-like textures, the local contrast disappears, when the incident illumination is parallel to the grooves. In consequence, the contrast in surface areas showing grooves has two maxima for the respective azimuth angles, whereas an anisotropic area has an approximately constant contrast. Evaluating such contrast features thus allows a robust classification of 3D-textures.

4. PARAMETER CHARACTERISTICS

The imaging parameters listed in Tab. 1 do not all have identical properties. Since the parameters result from different physical mechanisms, they show individual domains.

Some of the important parameters are cyclic or have a cyclic support. Among the position parameters of the illumination and observation, the azimuth angles ϕ_i and ϕ_e are cyclic themselves. Consequently, the image intensities taken with a fixed camera at a certain image point $I_\mathrm{c}(\boldsymbol{x},\phi_\mathrm{i})$ obtained when ϕ_i is varied is periodic with 2π.

When a moving camera together with a fixed illumination is to be considered, the camera causes a mapping of the surface $\boldsymbol{x}$ to the image position $\boldsymbol{x}_\mathrm{c} = (x_\mathrm{c}, y_\mathrm{c})^\mathrm{T}$:

$$\mathcal{M} : \boldsymbol{x} \mapsto \boldsymbol{x}_\mathrm{c} = \boldsymbol{A}\cdot\boldsymbol{x} + \boldsymbol{b}\,. \tag{6}$$

In case of a fixed camera orientation mentioned above, the camera observes the same object region, i. e. the projection parameters $\boldsymbol{A}$, $\boldsymbol{b}$ remain constant. For a moving camera, the mapping $\mathcal{M}$ changes with the angular coordinates θ_e and ϕ_e. The resulting mapping can be explicitly calculated from the camera angles θ_e and ϕ_e, if an analytic representations of the surface exists.[7] Variations of the camera orientation are advantageous for sensing the shape of the object (shape from stereo, shape from motion[11]). In many cases, objects are only accessible by taking multiple images with varying camera position.

For a surface inspection of an object, it is often advantageous to translate the observed intensity $I_\mathrm{c}(\boldsymbol{x}_\mathrm{c},\theta_\mathrm{e},\phi_\mathrm{e})$ back to the emitted surface radiance $L_\mathrm{e}(\boldsymbol{x},\theta_\mathrm{e},\phi_\mathrm{e})$ and to interpret it as a function of the surface coordinates $\boldsymbol{x}$ and the camera angles:

$$I_\mathrm{c}(\boldsymbol{x},\theta_\mathrm{e},\phi_\mathrm{e}) = I_\mathrm{c}\left(\boldsymbol{A}(\theta_\mathrm{e},\phi_\mathrm{e})^{-1}\big(\boldsymbol{x}_\mathrm{c} - \boldsymbol{b}(\theta_\mathrm{e},\phi_\mathrm{e})\big),\theta_\mathrm{e},\phi_\mathrm{e}\right) \propto \int_{\omega_\mathrm{c}} L_\mathrm{e}(\boldsymbol{x},\theta_\mathrm{e},\phi_\mathrm{e})\,\mathrm{d}\omega_\mathrm{c}\,, \tag{7}$$

where ω_c is the solid angle of the entrance pupil of the imaging lens seen from the surface point. For constant small angles ω_c, Eq. (7) can be simplified:

$$I_\mathrm{c}(\boldsymbol{x},\theta_\mathrm{e},\phi_\mathrm{e}) \propto L_\mathrm{e}(\boldsymbol{x},\theta_\mathrm{e},\phi_\mathrm{e})\,. \tag{8}$$

The recorded intensity $I_\mathrm{c}(\boldsymbol{x},\theta_\mathrm{e},\phi_\mathrm{e})$ for a certain surface point is thus proportional to the emitted radiance $L_\mathrm{e}(\boldsymbol{x},\theta_\mathrm{e},\phi_\mathrm{e})$.[8] Explicitly determining the exact projection parameters $\boldsymbol{A}(\theta_\mathrm{e},\phi_\mathrm{e})$, $\boldsymbol{b}(\theta_\mathrm{e},\phi_\mathrm{e})$ may be difficult in practice, since this would require an exact surface modelling or reconstruction. The main idea in our case is that for a variation of the azimuth ϕ_e, the projection parameters and hence the resulting camera intensities

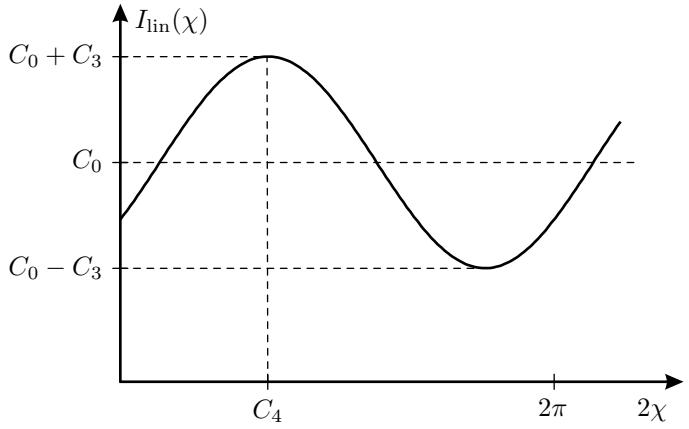

Figure 2. Variation of the intensity transmitted by a polarizer.

$I_{\mathrm{c}}(\boldsymbol{x}, \theta_{\mathrm{e}}, \phi_{\mathrm{e}})$ at a fixed surface point are cyclic with 2π and show the same characteristics as if the positions of the illumination and the camera are exchanged. This property also results directly from the reciprocity of the bidirectional reflectance distribution function (BRDF).[12]

The polarization state of a light beam is completely defined by three parameters (amplitudes $E_{\mathrm{i},\xi}$, $E_{\mathrm{i},\eta}$ and phase shift $\Delta\delta_{\mathrm{i}}$, or $E_{\mathrm{c},x}$, $E_{\mathrm{c},x}$, $\Delta\delta_{\mathrm{c}}$, resp.). To measure polarization, however, recordings have to be taken with a polarizer whose transmission axis is rotated by the variable angle χ to the ξ-axis. Passing through a linear polarizer, the transmitted intensity is*[13]

$$I_{\mathrm{lin}}(\chi) = E_{\mathrm{i},\xi}^2 \cos^2\chi + E_{\mathrm{i},\eta}^2 \sin^2\chi + E_{\mathrm{i},\xi} E_{\mathrm{i},\eta} \sin 2\chi \cos\Delta\delta_{\mathrm{i}} \tag{9}$$

$$= C_0 + C_1 \cos 2\chi + C_2 \sin 2\chi \tag{10}$$

$$= C_0 + \sqrt{C_1^2 + C_2^2} \cdot \cos\left(2\chi - \arctan\frac{C_2}{C_1}\right) \tag{11}$$

$$= C_0 + C_3 \cos(2\chi - C_4) \tag{12}$$

with

$$C_0 = \frac{1}{2}(E_{\mathrm{i},\xi}^2 + E_{\mathrm{i},\eta}^2)\,, \quad C_1 = \frac{1}{2}(E_{\mathrm{i},\xi}^2 - E_{\mathrm{i},\eta}^2)\,, \quad C_2 = E_{\mathrm{i},\xi} E_{\mathrm{i},\eta} \cos\Delta\delta_{\mathrm{i}} \quad \text{and} \tag{13}$$

$$C_3 = \sqrt{C_1^2 + C_2^2}\,, \quad C_4 = \arctan\frac{C_2}{C_1}\,. \tag{14}$$

C_0 is half of the intensity that is obtained without polarizer. C_3 and C_4 determine the amplitude and phase of the oscillation, see Fig. 2. In consequence, the resulting intensity for a rotated linear polarizer is a harmonic function with a π-cyclicity with respect to χ. Taking three measurements for different values of χ, the course of $I_{\mathrm{lin}}(\chi)$ is fully described and the constants C_0, C_3, C_4 (also C_1, C_2) and thus $E_{\mathrm{i},\xi}$, $E_{\mathrm{i},\eta}$ can be determined.

This calculation can be traced back to a linear system of equations, when Eq. (12) is written as[14]

$$I_{\mathrm{lin}}(\chi) = \boldsymbol{c}(\chi)^{\mathrm{T}} \cdot \boldsymbol{p} \tag{15}$$

with

$$\boldsymbol{c}(\chi) = (1,\, \cos 2\chi,\, \sin 2\chi)^{\mathrm{T}}\,, \quad \boldsymbol{p} = (C_0,\, C_3 \cos C_4,\, C_3 \sin C_4)^{\mathrm{T}}\,, \tag{16}$$

where $\boldsymbol{c}(\chi)$ depends on the given filter position and $\boldsymbol{p}$ denotes the desired quantities. When $n = 3$ measurements are taken, the system of n equations can be solved to obtain $\boldsymbol{p}$ and, in consequence, $E_{\mathrm{i},\xi}$ and $E_{\mathrm{i},\eta}$. For more than

*The principle of measurement is demonstrated with the illuminating light (index i), but can be transferred analogously to the observed light.

3 measurements, the over-determination of the resulting equation system can be used to make the estimation of $\boldsymbol{p}$ more robust, e. g. in the sense of a least squares (LS) estimation.

However, from Eq. (13), it can be seen that for $\Delta\delta_\mathrm{i}$, only the absolute value can be determined. This is due to the cos-function, which is an even function. Even if more than three measurements with additional values of χ were taken, the uncertainty concerning the sign of $\Delta\delta_\mathrm{i}$ remains.

The common way to overcome this issue is to use additional measurements with a circular polarizer obtained by adding a $\frac{\pi}{2}$-retarder, which causes a delay of one component, e. g. the η-component. The intensity then obtained is

$$I_\mathrm{circ}(\chi) = E_{\mathrm{i},\xi}^2 \cos^2\chi + E_{\mathrm{i},\eta}^2 \sin^2\chi + E_{\mathrm{i},\xi} E_{\mathrm{i},\eta} \sin 2\chi \sin\Delta\delta_\mathrm{i} \tag{17}$$

$$= D_0 + D_1 \cos 2\chi + D_2 \sin 2\chi \;, \tag{18}$$

where

$$D_0 = C_0 \;, \quad D_1 = C_1 \quad \text{and} \quad D_2 = E_{\mathrm{i},\xi} E_{\mathrm{i},\eta} \sin\Delta\delta_\mathrm{i} \;. \tag{19}$$

Since the sin-function is an odd function and all other constants are known from the recordings with the linear polarizer, the missing sign of $\Delta\delta_\mathrm{i}$ is obtained with a single measurement using the circular polarizer.[†]

In consequence, at least four measurements have to be carried out to obtain the Stokes vector characterizing the light beam and to perform the Mueller calculus.[5] Since the curve of the intensity transmitted through a polarizer only contains the first harmonic component, the Stokes vector with its four components fully describes the polarization state of a light beam. It can be used instead of the oscillation amplitudes E_ξ, E_η and the phase difference $\Delta\delta$.

5. SURFACE MODELLING

The interaction between the illumination and the object leads to a modulation of the re-emitted light, which can be the base for an object or surface classification. This modification may concern all light properties enumerated in Sect. 4. Among them, the most important surface characteristics are contained in the directional distribution of the reflected radiance L_e, which can be described through the BRDF[15]

$$f_\mathrm{r}(\theta_\mathrm{i}, \phi_\mathrm{i}, \theta_\mathrm{e}, \phi_\mathrm{e}) = \frac{L_\mathrm{e}(\theta_\mathrm{i}, \phi_\mathrm{i}, \theta_\mathrm{e}, \phi_\mathrm{e})}{E_\mathrm{i}(\theta_\mathrm{i}, \phi_\mathrm{i})} \;. \tag{20}$$

The BRDF is an empirical quantity which depends on the directions of the incident and the emitted light. Consequently, modelling the BRDF can be useful to find suitable sampling demands for the illumination and observation angles. It has been established that for many technically relevant surfaces, a model containing different types of reflection is appropriate.[16] The BRDF can then be expressed as

$$f_\mathrm{r} = \mu_\mathrm{spec} f_\mathrm{spec}(\boldsymbol{e}_\mathrm{i}, \boldsymbol{e}_\mathrm{e}, \boldsymbol{e}_\mathrm{n}) + \mu_\mathrm{fsc} f_\mathrm{fsc}(\boldsymbol{e}_\mathrm{i}, \boldsymbol{e}_\mathrm{e}, \boldsymbol{e}_\mathrm{n}) + \mu_\mathrm{Lamb} f_\mathrm{Lamb} + \mu_\mathrm{bsc} f_\mathrm{bsc}(\boldsymbol{e}_\mathrm{i}, \boldsymbol{e}_\mathrm{e}, \boldsymbol{e}_\mathrm{n}) \tag{21}$$

with the dimensionless constants μ_i to weight the components f_i:

$$f_\mathrm{spec}(\boldsymbol{e}_\mathrm{i}, \boldsymbol{e}_\mathrm{e}, \boldsymbol{e}_\mathrm{n}) = F(\boldsymbol{e}_\mathrm{s}, \boldsymbol{e}_\mathrm{n}, \eta) \frac{\delta_\omega(\boldsymbol{e}_\mathrm{n} - \boldsymbol{e}_\mathrm{s})}{2\boldsymbol{e}_\mathrm{i}^\mathrm{T}\boldsymbol{e}_\mathrm{n}} = F(\boldsymbol{e}_\mathrm{s}, \boldsymbol{e}_\mathrm{n}, \eta) \frac{\delta(\theta_\mathrm{i} - \theta_\mathrm{e})\; \delta(|\phi_\mathrm{i} - \phi_\mathrm{e}| - \pi)}{\sin\theta_\mathrm{i}\; \cos\theta_\mathrm{i}} \;, \tag{22}$$

$$f_\mathrm{fsc}(\boldsymbol{e}_\mathrm{i}, \boldsymbol{e}_\mathrm{e}, \boldsymbol{e}_\mathrm{n}) = \zeta_\mathrm{fsc} S(\boldsymbol{e}_\mathrm{i}, \boldsymbol{e}_\mathrm{e}, \boldsymbol{e}_\mathrm{n}) F(\boldsymbol{e}_\mathrm{s}, \boldsymbol{e}_\mathrm{n}, \eta) \frac{\Phi(\boldsymbol{e}_\mathrm{s}^\mathrm{T}\boldsymbol{e}_\mathrm{n})}{(\boldsymbol{e}_\mathrm{i}^\mathrm{T}\boldsymbol{e}_\mathrm{n})(\boldsymbol{e}_\mathrm{e}^\mathrm{T}\boldsymbol{e}_\mathrm{n})} \;, \tag{23}$$

$$f_\mathrm{Lamb} = \frac{1}{\pi} \;, \tag{24}$$

$$f_\mathrm{bsc}(\boldsymbol{e}_\mathrm{i}, \boldsymbol{e}_\mathrm{e}, \boldsymbol{e}_\mathrm{n}) = \zeta_\mathrm{bsc} S(\boldsymbol{e}_\mathrm{i}, \boldsymbol{e}_\mathrm{e}, \boldsymbol{e}_\mathrm{n}) \frac{p(\boldsymbol{e}_\mathrm{i}^\mathrm{T}\boldsymbol{e}_\mathrm{e})}{(\boldsymbol{e}_\mathrm{i}^\mathrm{T}\boldsymbol{e}_\mathrm{n})(\boldsymbol{e}_\mathrm{e}^\mathrm{T}\boldsymbol{e}_\mathrm{n})} \;. \tag{25}$$

[†]An alternative way of measuring the Stokes parameters uses an isotropic filter instead of the third setting of the linear polarizer.

For the *specular component* f_{spec}, the specular reflection law is defined with the Dirac delta distribution for solid angles

$$\delta_\omega(\boldsymbol{\omega}) = \delta_\omega(\theta - \theta_0, \phi - \phi_0) = \frac{\delta(\theta - \theta_0)\ \delta(\phi - \phi_0)}{\sin\theta_0}\ , \tag{26}$$

where $\delta(.)$ is the standard Dirac delta distribution. $F(.)$ is the Fresnel reflectivity with the complex index of refraction η.[5] $\boldsymbol{e}_{\mathrm{s}}$ stands for the surface normal of the principal plane that leads to a specular reflection between $\boldsymbol{e}_{\mathrm{i}}$ and $\boldsymbol{e}_{\mathrm{e}}$:

$$\boldsymbol{e}_{\mathrm{s}} = \frac{\boldsymbol{e}_{\mathrm{i}} + \boldsymbol{e}_{\mathrm{e}}}{\|\boldsymbol{e}_{\mathrm{i}} + \boldsymbol{e}_{\mathrm{e}}\|}\ . \tag{27}$$

The *forescattering component* f_{fsc} contains a usually isotropic modelling of the distribution of the facet inclination (see e. g. Refs. 17, 18) used to define $\Phi(.)$, which is a monotonically increasing function with respect to its argument. $S(.)$ is the bistatic shadowing function which models the combined effects of shadowing and occlusion.[19] Such effects may become important for grazing or reflecting angles. ζ_{fsc} is a normalizing constant such that the remaining expression has the dimensions of a BRDF.

The *Lambertian component* f_{Lamb} is constant for any direction of observation $\boldsymbol{e}_{\mathrm{e}}$.[8] Since Lambertian reflection is dominated by body reflection which destroys polarization, this term does not contain a Fresnel factor.

The *backscatter lobe* f_{bsc} is obtained from the phase function $p(.)$. The phase function is modelled according to the type of the scattering surface.[19] ζ_{bsc} is again a constant ensuring the correct dimension of the expression for f_{bsc}.

5.1. Specular reflection

In the case of a very smooth object surface, specular reflection dominates. The BRDF is then

$$f_{\mathrm{r}} = f_{\mathrm{spec}}(\boldsymbol{e}_{\mathrm{i}}, \boldsymbol{e}_{\mathrm{e}}, \boldsymbol{e}_{\mathrm{n}}) = F(\boldsymbol{e}_{\mathrm{s}}, \boldsymbol{e}_{\mathrm{n}}, \eta)\frac{\delta_\omega(\boldsymbol{e}_{\mathrm{n}} - \boldsymbol{e}_{\mathrm{s}})}{2\boldsymbol{e}_{\mathrm{i}}^{\mathrm{T}}\boldsymbol{e}_{\mathrm{n}}}\ . \tag{28}$$

The delta function in Eq. (28) describes a small peak area of the registered intensity in the four-dimensional angular space (θ_{i}, θ_{e}, ϕ_{i}, ϕ_{e}), when the illumination or camera angles are varied and $\boldsymbol{e}_{\mathrm{n}} = \boldsymbol{e}_{\mathrm{s}}$. In addition, significant variations of the recorded image intensities can be expected, when the polarization state of the incident illumination or the emitted light is considered, see Sect. 4. The occurrence of a single peak in the BRDF $f_{\mathrm{r}}(\theta_{\mathrm{i}}, \theta_{\mathrm{e}}, \phi_{\mathrm{i}}, \phi_{\mathrm{e}})$ makes it very difficult to justify a certain sampling pattern in the angular space. In theory, an adequate sampling is impossible due to the vanishing extension of the δ-peak.

Fortunately, real measurement equipments usually cause low-pass filtering on the illumination distribution and the detector response $I_{\mathrm{c}}(\boldsymbol{x}, \theta_{\mathrm{e}}, \phi_{\mathrm{e}})$. When ideal point light sources are replaced by area light sources, high frequency components in $E_{\mathrm{i}}(\theta_{\mathrm{i}}, \phi_{\mathrm{i}})$ are reduced. The finite aperture of the camera also causes a low-pass effect on $I_{\mathrm{c}}(\boldsymbol{x}, \theta_{\mathrm{e}}, \phi_{\mathrm{e}})$. Taking into account the reciprocity of illumination and detector, the solid angle of the camera aperture is equivalent to a low-pass filtering of a point light source which corresponds to an area light source with the same solid angle.[20] In consequence, it is not indicated to increase the sampling rate of the angular spaces of the illumination or the observation over a certain level.

An example will explain this connection:[20] For a reproduction scale of $1:1$, the entrance pupil of the camera with an aperture stop of K fills the solid angle $\frac{\pi}{16K^2}$. When this solid angle is related to the solid angle 2π of the half space of all possible illuminations, a number of $N = 32K^2$ light sources is obtained. Consequently, when the half space of the illuminations is sampled with N discriminable light sources at equidistant illumination angles, no substantial sampling error is committed.

5.2. Diffuse reflection

For a surface without specular reflection component, the BRDF reduces to

$$f_{\mathrm{r}} = \mu_{\mathrm{fsc}}\zeta_{\mathrm{fsc}}S(\boldsymbol{e}_{\mathrm{i}}, \boldsymbol{e}_{\mathrm{e}}, \boldsymbol{e}_{\mathrm{n}})F(\boldsymbol{e}_{\mathrm{s}}, \boldsymbol{e}_{\mathrm{n}}, \eta)\frac{\Phi(\boldsymbol{e}_{\mathrm{s}}^{\mathrm{T}}\boldsymbol{e}_{\mathrm{n}})}{(\boldsymbol{e}_{\mathrm{i}}^{\mathrm{T}}\boldsymbol{e}_{\mathrm{n}})(\boldsymbol{e}_{\mathrm{e}}^{\mathrm{T}}\boldsymbol{e}_{\mathrm{n}})} + \mu_{\mathrm{Lamb}}\frac{1}{\pi} + \mu_{\mathrm{bsc}}\zeta_{\mathrm{bsc}}S(\boldsymbol{e}_{\mathrm{i}}, \boldsymbol{e}_{\mathrm{e}}, \boldsymbol{e}_{\mathrm{n}})\frac{p(\boldsymbol{e}_{\mathrm{i}}^{\mathrm{T}}\boldsymbol{e}_{\mathrm{e}})}{(\boldsymbol{e}_{\mathrm{i}}^{\mathrm{T}}\boldsymbol{e}_{\mathrm{n}})(\boldsymbol{e}_{\mathrm{e}}^{\mathrm{T}}\boldsymbol{e}_{\mathrm{n}})}\ . \tag{29}$$

In practical applications, some of the components can be neglected and lead to a considerable simplification of Eq. (29): The bistatic shadowing function $S(\boldsymbol{e}_\mathrm{i}, \boldsymbol{e}_\mathrm{e}, \boldsymbol{e}_\mathrm{n})$ is nearly constant over a large range of non-grazing polar angles θ_i, θ_e. The portion of the backscattering component is usually rather small, which makes it reasonable to neglect the respective term. In the following considerations, an isotropic surface texture and a non-polarized illumination is assumed.

Using the Torrance-Sparrow reflection model,[18] the forescattering component becomes then

$$f_\mathrm{fsc}(\boldsymbol{e}_\mathrm{i}, \boldsymbol{e}_\mathrm{e}, \boldsymbol{e}_\mathrm{n}) \propto \frac{F(\theta'_\mathrm{i}, n)\, \exp\left(-c^2\alpha^2\right)}{\cos\theta_\mathrm{i} \cos\theta_\mathrm{e}} \tag{30}$$

with

$$F(\theta'_\mathrm{i}, n) \propto r_\perp^2(\theta'_\mathrm{i}, n) + r_\parallel^2(\theta'_\mathrm{i}, n) = \left(\frac{a - \cos\theta'_\mathrm{i}}{a + \cos\theta'_\mathrm{i}}\right)^2 \left(1 + \left(\frac{a - \sin\theta'_\mathrm{i} \tan\theta'_\mathrm{i}}{a + \sin\theta'_\mathrm{i} \tan\theta'_\mathrm{i}}\right)^2\right) , \tag{31}$$

$$\theta'_\mathrm{i} = \frac{1}{2} \cos^{-1}\left(\cos\theta_\mathrm{e} \cos\theta_\mathrm{i} - \sin\theta_\mathrm{e} \sin\theta_\mathrm{i} \cos(\Delta\phi - \pi)\right) , \tag{32}$$

$$\alpha = \cos^{-1}\left(\cos\theta_\mathrm{i} \cos\theta'_\mathrm{i} + \sin\theta_\mathrm{i} \sin\theta'_\mathrm{i} \cos\beta\right) , \tag{33}$$

$$\beta = \sin^{-1}\left(\frac{\sin(\Delta\phi - \pi) \sin\theta_\mathrm{e}}{\sin 2\theta'_\mathrm{i}}\right) , \tag{34}$$

$$a = \sqrt{n^2 - \sin^2\theta_\mathrm{i}} , \quad \Delta\phi = \phi_\mathrm{e} - \phi_\mathrm{i} . \tag{35}$$

n is the index of refraction, c is an attenuation factor in the surface model used by Torrance-Sparrow.

Fig. 3 shows the normalized forescattering component f_fsc in relation to $\Delta\phi$ for variations of θ_i, θ_e, n and c. In addition, a cosine function is depicted (thin dotted line). It can be seen that the modelled BRDF component essentially resembles the cosine function. An important observation is that moderate variations of the model parameters and of the imaging parameters do not considerably alter the course of $f_\mathrm{fsc}(\Delta\phi)$. This makes it possible to justify that in order to describe the intensity dependence on $\Delta\phi$ for classification tasks, only the dominating first harmonic component of $f_\mathrm{fsc}(\Delta\phi)$ has to be taken into account. Consequently, only few more than 3 measurements have to be taken. A very similar result is obtained when the polar angles θ_i or θ_e are considered. In this case, however, the non-cyclic support of the polar angles have to be taken into account.

6. CONCLUSION

Sampling the parameter space in image series is a complex topic: The parameter domain comprises more than 20 parameters with individual properties, which all are useful to characterize a surface and thus can be used for a surface classification. A theoretical derivation of the sampling conditions for the domains of several important parameters is difficult to handle. Whereas the spectral properties of some parameters, e. g. the polarization state of the incident beam on the surface and the re-emitted beam, can be fully described through the underlying physics and is constant for all surfaces, other parameters lead to intensity functions on the sensor, the spectra of which depend on the object in question. Mainly the reflection properties of the surface can cause intensity characteristics with high frequencies, resulting in sampling instructions which are highly dependent on previous knowledge. A promising approach of treating the sampling issue can therefore be developed starting with suitable models of the surface reflection. That way, practical sampling instructions, which are useful in many applications, are obtained.

REFERENCES

1. C. E. Shannon, "Communication in the presence of noise (classic paper)," *Proc. of the IEEE* **86**(2), pp. 447–457, 1998.
2. M. Unser, "Sampling—50 years after Shannon," *Proc. of the IEEE* **88**(4), pp. 569–587, 2000.
3. E. Kreyszig, *Introductory Functional Analysis with Applications*, John Wiley & Sons, New York, 1978.

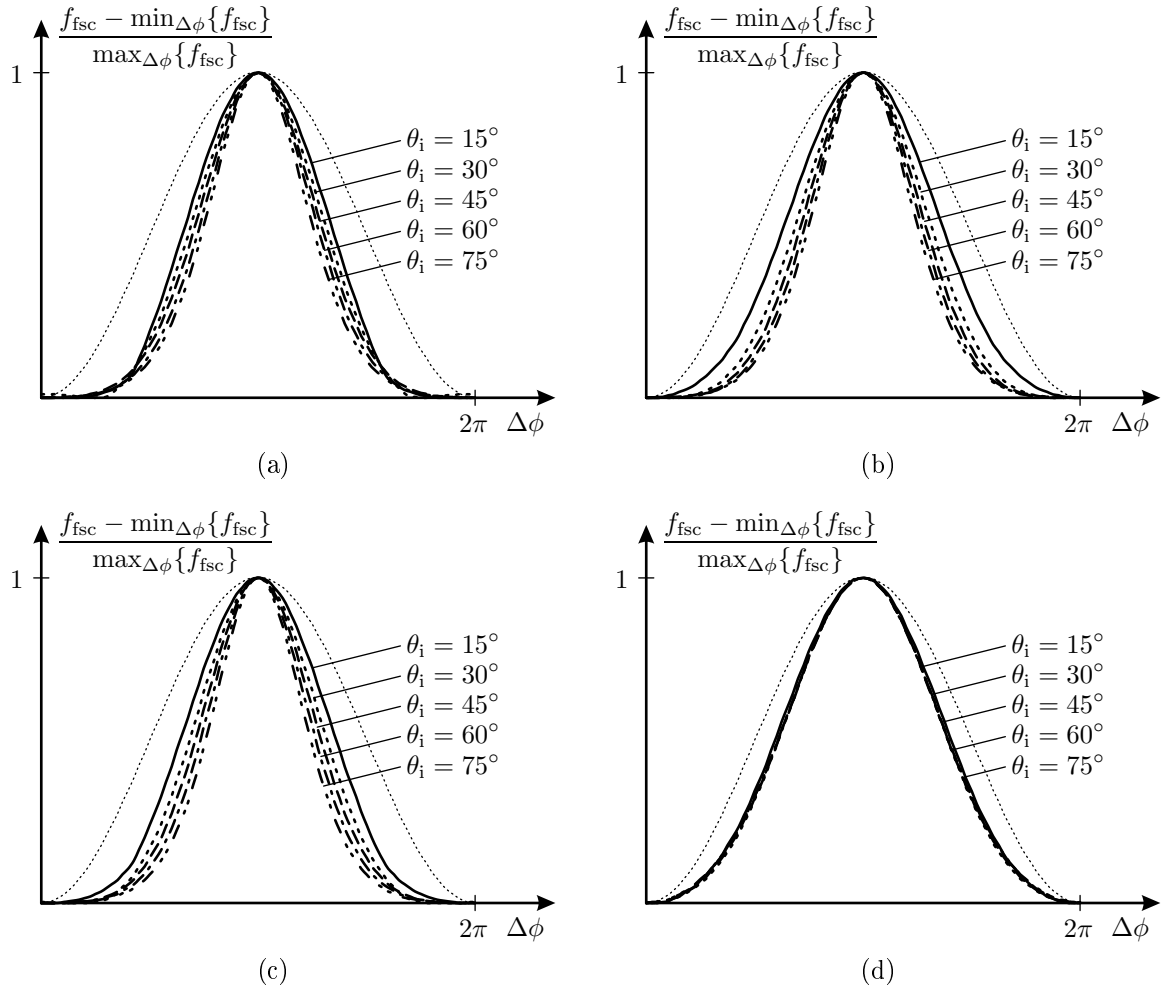

Figure 3. Normalized forescattering component f_{fsc}: (a) $\theta_{\mathrm{e}} = 45°$, $n = 1.5$, $c = 0.15$; (b) $\theta_{\mathrm{e}} = 45°$, $n = 1.5$, $c = 0.05$; (c) $\theta_{\mathrm{e}} = 45°$, $n = 1.2$, $c = 0.15$; (d) $\theta_{\mathrm{e}} = 15°$, $n = 1.5$, $c = 0.15$.

4. J. R. Higgins, *Sampling Theory in Fourier and Signal Analysis*, Clarendon Press, Oxford, 1996.
5. M. Born and E. Wolf, *Principles of Optics*, Cambridge University Press, Cambridge, 7 ed., 1999.
6. E. Hecht, *Optics*, Addison Wesley, San Francisco (CA), 4 ed., 2002.
7. E. Trucco and A. Verri, *Introductory Techniques for 3-D Computer Vision*, Prentice Hall, Upper Saddle River (NJ), 1998.
8. B. K. P. Horn and M. J. Brooks, eds., *Shape from Shading*, MIT Press, Cambridge (MA), 1989.
9. R. Woodham, "Photometric stereo: A reflectance map technique for determining surface orientation from image intensity," in *Image Understanding Systems and Industrial Applications, Proc. of SPIE* **155**, pp. 136–143, SPIE, 1978.
10. M. Heizmann, "Segmentation of striation patterns using illumination series," in *Photonics in Measurement*, T. Pfeifer and R. Tutsch, eds., *VDI-Berichte* **1844**, pp. 461–470, VDI, 2004.
11. B. K. P. Horn, ed., *Robot Vision*, MIT Press, Cambridge (MA), 1986.
12. W. C. Snyder, "Reciprocity of the bidirectional reflectance distribution function (brdf) in measurements and models of structured surfaces," *IEEE Transactions on Geoscience and Remote Sensing* **36**(2), pp. 685–691, 1998.
13. D. Clarke and J. F. Grainger, *Polarized Light and Optical Measurement*, Pergamon Press, Oxford, 1971.

14. S. K. Nayar, X.-S. Fang, and T. Boult, "Separation of reflection components using color and polarization," *International Journal of Computer Vision* **21**(3), pp. 163–186, 1997.
15. F. E. Nicodemus, J. C. Richmond, J. J. Hsia, I. W. Ginsberg, and T. Limperis, "Geometrical considerations and nomenclature for reflectance," NBS Monograph 160, National Bureau of Standards, U.S. Department of Commerce, Washington (DC), 1977.
16. H. D. Tagare and R. J. P. deFigueiredo, "A theory of photometric stereo for a class of diffuse non-lambertian surfaces," *IEEE Transactions on Pattern Analysis and Machine Intelligence* **13**(2), pp. 133–152, 1991.
17. B. T. Phong, "Illumination for computer generated pictures," *Communications of the ACM* **18**(6), pp. 311–317, 1975.
18. K. E. Torrance and E. M. Sparrow, "Theory for off-specular reflection from roughened surfaces," *Journal of the Optical Society of America* **57**(9), pp. 1105–1114, 1967.
19. H. D. Tagare and R. J. P. deFigueiredo, "A framework for the construction of reflectance maps for machine vision," *CVGIP: Image Understanding* **57**(3), pp. 265–282, 1993.
20. R. W. Malz, *Codierte Lichtstrukturen für 3D-Meßtechnik und Inspektion*. PhD thesis, Universität Stuttgart, 1992.